JGR Solid Earth

RESEARCH ARTICLE
10.1029/2019JB019315

Key Points:
- We testified the control of lithospheric thickness on the compositional variation of continental intraplate basalts
- Basalts record faithfully only the final depth of melting or melt equilibration
- A melt rich layer close beneath the lithosphere-asthenosphere boundary is a possible site for crystallizing clinopyroxene megacrysts

Supporting Information:
- Supporting Information S1

Correspondence to:
P. Sun and Y. Niu,
pu.sun@qdio.ac.cn;
yaoling.niu@durham.ac.uk

Citation:
Sun, P., Niu, Y., Guo, P., Duan, M., Wang, X., Gong, H., & Xiao, Y. (2020). The lithospheric thickness control on the compositional variation of continental intraplate basalts: A demonstration using the Cenozoic basalts and clinopyroxene megacrysts from eastern China. *Journal of Geophysical Research: Solid Earth*, *125*, e2019JB019315. https://doi.org/10.1029/2019JB019315

Received 29 DEC 2019
Accepted 2 MAR 2020
Accepted article online MAR 03 2020

The Lithospheric Thickness Control on the Compositional Variation of Continental Intraplate Basalts: A Demonstration Using the Cenozoic Basalts and Clinopyroxene Megacrysts From Eastern China

Pu Sun[1,2], Yaoling Niu[2,3,4], Pengyuan Guo[1,2], Meng Duan[1,2], Xiaohong Wang[1,2], Hongmei Gong[1,2], and Yuanyuan Xiao[1,2]

[1]Key Laboratory of Marine Geology and Environment, Institute of Oceanology, Chinese Academy of Sciences, Qingdao, China, [2]Laboratory for Marine Geology, Qingdao National Laboratory for Marine Science and Technology, Qingdao, China, [3]Department of Earth Sciences, Durham University, Durham, UK, [4]School of Earth Science and Resources, China University of Geosciences, Beijing, China

Abstract Studies on intraplate ocean island basalts have demonstrated the control of lithosphere thickness on the extent of melting and pressure of melt extraction (i.e., the lid effect). However, whether lithosphere thickness also controls the composition of within-continent basalts remains unclear. Here, we test this hypothesis by studying the Cenozoic basalts containing clinopyroxene megacrysts from 10 localities throughout eastern continental China with a north-south spatial coverage in excess of 2,500 km. Indeed, the geochemical parameters (e.g., abundances and ratios of major and trace elements) correlate well with the depth of the lithosphere-asthenosphere boundary (LAB) calculated using the clinopyroxene barometry, showing significant lithospheric thickness control on basalt compositions. These observations offer further evidence for melt pooling (a melt rich layer) close beneath the LAB as a "stable magma reservoir" for crystallizing compositionally uniform clinopyroxene megacrysts to be carried by subsequent pulses of melt transport and eruption.

Plain Language Summary Magmas erupted on the surface of Earth have different compositions. These compositional variations may result from mantle source compositional variations, varying extent and pressure of melting as well as magma evolution during ascent. Studies have observed significant control of oceanic lithospheric thickness on the compositional variation of oceanic basalts. Magmas erupted on thick lithosphere have geochemical signatures of high pressure and low extent of melting, whereas magmas erupted on thin lithosphere have signatures of low pressure and high extent of melting. However, whether continental lithospheric thickness has similar compositional control on the within-continent basalts remains unclear, largely because the continental lithosphere thickness at the time of volcanism is unknown. In this study, we test this hypothesis by studying the Cenozoic basalts containing clinopyroxene megacrysts from 10 localities throughout eastern continental China with a north-south spatial coverage in excess of 2,500 km. These clinopyroxene megacrysts were explained as high-pressure cumulates from basaltic magmas at sites close to the base of the lithosphere, and their equilibrium pressures (depths) calculated using the clinopyroxene geobarometer are thus ideal proxies for the lithosphere thickness at the time of eruptions. This study demonstrated significant control of continental lithospheric thickness on the compositional variation of within-continent magmas.

1. Introduction

Intraplate basalts vary in composition as a result of mantle source heterogeneity, varying extent and pressure of melting as well as magma evolution and assimilation during ascent at shallow levels. Studies on intraplate ocean island basalts (OIB) have confirmed these mechanisms (e.g., Helz, 1987; Niu et al., 2011, 2012; White & Hofmann, 1982; Zindler & Hart, 1986) and demonstrated that the effect of pressure and extent of melting is largely controlled by lithosphere thickness at the time of volcanism (i.e., the lid effect; Haase, 1996; Humphreys & Niu, 2009; Niu et al., 2011). OIB erupted on thick lithosphere have geochemical characteristics of low extent (F) and high pressure (P) of melting with a strong garnet signature (e.g., low SiO_2, Al_2O_3,

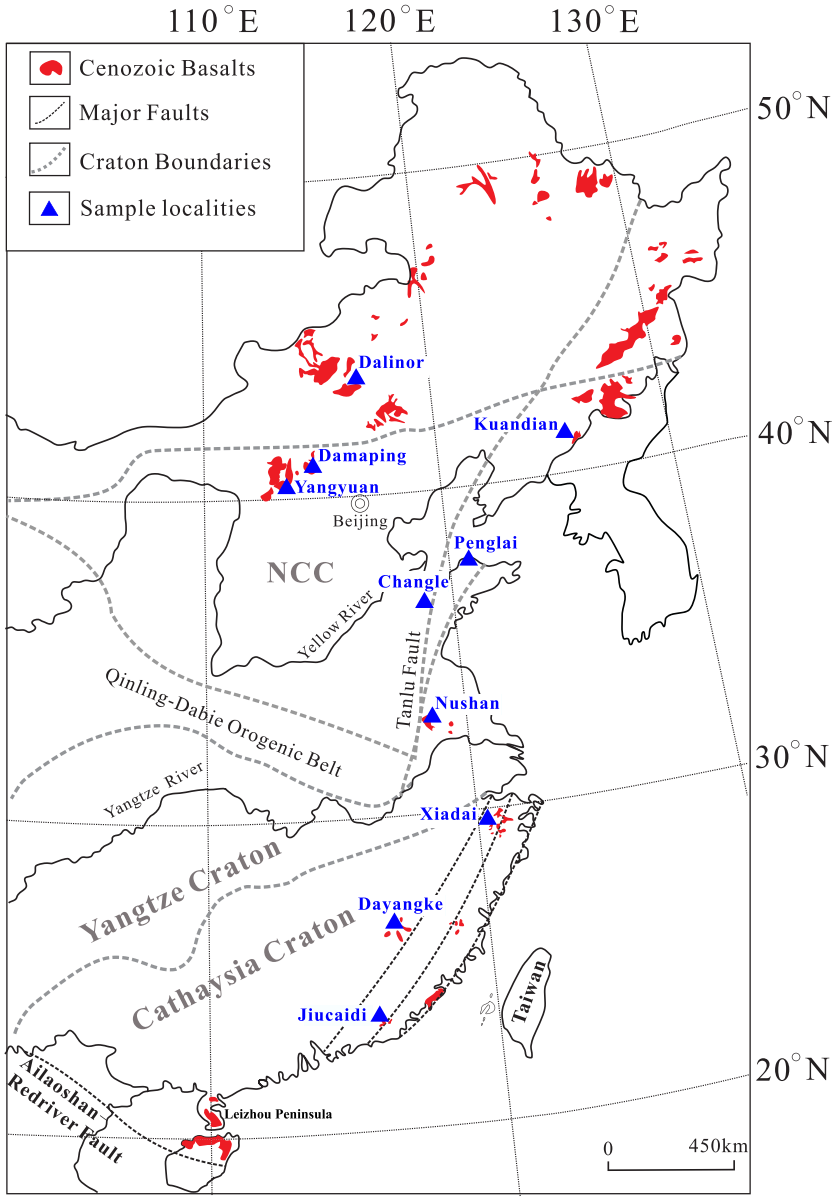

Figure 1. Distribution of the Cenozoic volcanism and 10 locations of our cpx megacryst-bearing basalt samples dispersed in the entire eastern continental China (modified from Sun et al., 2017).

and high FeO, MgO, TiO_2, P_2O_5, and Sm/Yb), whereas those erupted on thin lithosphere exhibit the reverse, that is, a high F and low P of melting with a weak garnet signature (e.g., high SiO_2, Al_2O_3, and low FeO, MgO, TiO_2, P_2O_5 and Sm/Yb) (Niu et al., 2011).

In terms of understood mechanisms of mantle melting and melt extraction, it is expected that lithosphere thickness variation should also control the composition of within-continent basalts as previously hypothesized based on a few studies (e.g., Davies et al., 2015; Guo et al., 2019; Sun et al., 2017). However, this hypothesis has not been rigorously tested because unlike the oceanic lithosphere whose thickness (L) can be well estimated from its age (t) by the half-space cooling model (HSM) $L \propto t^{1/2}$ (e.g., Parsons & McKenzie, 1978; Sclater & Francheteau, 1970), the continental lithosphere thickness at the time of volcanism is unknown.

Eastern continental China is ideal for testing this hypothesis because this vast region (1) experienced significant lithosphere thinning in the late Mesozoic, resulting in a variably thinned Cenozoic lithosphere (~60–100 km) (e.g., Chen et al., 2008; Gao et al., 2004; Griffin et al., 1998; Menzies et al., 1993;

Niu, 2005; Niu et al., 2015), and (2) underwent volumetrically small, but widespread basaltic volcanism in the Cenozoic (Figure 1; e.g., Basu et al., 1991; Chen, 2009; Chen et al., 2008; Fan & Hooper, 1991; Liu et al., 1994; Guo et al., 2016; Song et al., 1990; Sun et al., 2017, 2018; Zou et al., 2000). Moreover, clinopyroxene megacrysts which are commonly observed in the worldwide alkali basalts (Akinin et al., 2005; Chapman, 1976; Chin, 2018; Dobosi & Jenner, 1999; Irving, 1974; Irving & Frey, 1984; Richter & Carmichael, 1993; Shaw & Eyzaguirre, 2000; Woodland & Jugo, 2007) are abundant in the Cenozoic alkali basalts of eastern China. Previous studies usually explained the clinopyroxene megacrysts as high-pressure cumulates cognate with their host basalts (e.g., Irving & Frey, 1984) or disaggregated mantle crystals (i.e., xenocrysts; Richter & Carmichael, 1993; Chin, 2018). The clinopyroxene megacrysts in eastern China have been explained as high-pressure cumulates from basaltic magmas. However, these clinopyroxene megacrysts are not in equilibrium with their host basalts but are xenocrysts captured by their host basalts during ascent (Chen et al., 1997, 2009; Liu et al., 1992; Liu & Ying, 2019). In addition, calculations using clinopyroxene thermobarometers have revealed the origin of these clinopyroxene megacrysts at sites close to the base of the lithospheric mantle (Chen et al., 2009; Yu et al., 2019). If this is true, the equilibrium pressures (depths) of clinopyroxene megacrysts would be ideal proxies for the lithosphere thickness at the time of eruptions, which can thus be used jointly with the basalt compositions to test the lid effect in the intracontinent setting. In this study, we test this hypothesis by studying the Cenozoic alkali basalts containing clinopyroxene megacrysts throughout eastern continental China (Figure 1). We show that the lithospheric thickness (calculated using the clinopyroxene barometry) has significant control on the compositional variations of these basalts. On the other hand, basalts cannot record pressure information deeper than the base of lithosphere, because of efficient melt-solid equilibration on crystal grain-size scales during melt migration and aggregation in the asthenosphere (Niu, 2016; Niu et al., 2011). We also show that melt pooling (a melt rich layer) close beneath the lithosphere-asthenosphere boundary (LAB) as a "stable magma reservoir" is required to crystallize compositionally uniform clinopyroxene megacrysts entrained in these basalts. The latter offers a new insight into mantle melting and melt aggregation processes for continental basaltic magmatism.

2. Cenozoic Basaltic Volcanisms in Eastern China

Most of the Cenozoic basalts in eastern China are distributed along or adjacent to NNE-oriented regional faults (e.g., the Tanlu fault; Figure 1). These basalts are alkalic in composition (supporting information Figure S1) and have high abundances of incompatible elements with trace element patterns similar to that of present-day average OIB (Figure S2), which is best interpreted as reflecting a highly enriched mantle source (Basu et al., 1991; Fan & Hooper, 1991; Guo et al., 2016; Liu et al., 1994; Niu, 2005; Song et al., 1990; Sun et al., 2017; Zou et al., 2000). The widespread occurrence of mantle xenoliths in these basalts indicates a rapid ascend and limited crustal contamination (e.g., Zou et al., 2000). Clinopyroxene (cpx) megacrysts are common in these basalts and are black in hand specimen and optically homogeneous (Figure S3). They are usually anhedral and show vitreous appearance and conchoidal fracture with poor cleavage (Figure S3), similar to the cpx megacrysts found in the alkali basalts in south Australia (Irving, 1974) and Scotland (Chapman, 1976). In this study, cpx megacrysts-borne Cenozoic basalts from 10 localities dispersed in entire eastern continental China with a north-south spatial coverage in excess of 2,500 km have been studied to assess the possible influence of continental lithosphere thickness on the compositional variation of these intraplate basalts. Detailed erupting ages of these basalts are compiled in Table S2. Basalts from northeast China with rare cpx megacrysts (e.g., Chen et al., 2017; Zhang et al., 1995) and basalts from the Leizhou Peninsula and Hainan Island (Figure 1) showing extreme mantle source heterogeneity possibly influenced by the Hainan mantle plume (Flower et al., 1992; Sun et al., 2019; Tu et al., 1991; X. Wang, Li, et al., 2011) are not included here.

3. Data and Methods

We analyzed major and trace elements on 65 basalt samples and 47 cpx megacrysts from eastern China and also compiled data on cpx megacrysts and their host basalts in the literature. See supporting information for detailed analytical methods and Table S1–S6 for our new data and the literature data.

3.1. Correction for Fractionation Effect to Melt $Mg^{\#} = 72$

In order to explore the influence of lithospheric thickness on the compositions of these basalts, we need to correct for the effect of shallow-level fractionation on the major element compositions of these basalts to $Mg^{\#} = 72$ because basaltic melts with $Mg^{\#} \geq 72$ are in equilibrium with mantle olivine of Fo $\geq \sim 90$ (Roeder & Emslie, 1970).

There are two methods for such correction. The first one is to move the major element compositions back-tracked to $Mg^{\#} = 72$ along a set of LLDs (liquid lines of decent, which represents the chemical changes during fractional crystallization of basaltic magmas) (e.g., Niu et al., 1999; Niu & O'Hara, 2008). The shape of LLDs is determined by the order of appearance and proportions of liquidus phases (olivine, clinopyroxene, plagioclase, etc.), which are further determined by the composition of primitive magmas and crystallization conditions (e.g., pressure) (Green & Ringwood, 1967; O'Hara, 1965; Yoder, 1965). Using a set of LLDs derived from a large data set of MORBs, Niu et al. (1999) first used this method and corrected the major element compositions of MORB samples for the fractionation effect. However, compared with MORBs extracted at shallow depth with LLDs characterized by crystallization order of Ol → Ol + Pl → Pl + Cpx + Ol, the continental basalts extracted beneath the thickened lithosphere would have LLDs defined by crystallization order of Ol → Ol + Cpx → Cpx + Pl + Ol (Niu, 2005). In this case, we can follow Humphreys and Niu (2009) to effectively use the LLDs from Kilauea Iki Lava Lake of Hawaii OIB (erupted from thickened lithosphere; Helz, 1987) in our fractionation corrections. This is because (1) olivine and cpx are common liquidus phases for both OIB and Cenozoic basalts in eastern China and (2) eastern China and Hawaii have comparable lithospheric thickness of 60–100 km (e.g., An & Shi, 2006; Chen et al., 2006, 2008) and ~90 km (Humphreys & Niu, 2009), respectively, which determines similar melt extraction pressures and primitive melt compositions with comparable LLDs (Niu et al., 2011; Sun et al., 2017). Such correction may not be perfect because after all, the lithosphere thickness beneath the 10 sample localities are not the same, but the similar LLD mineral sequence (e.g., Ol → Ol + Cpx → Cpx + Pl + Ol) ensures the correction to be adequate approximation. The corrected data (with subscript 72-*LLD*; "72-*LLD* values") are given in Table S3 with the effectiveness of the correction shown by the total of 99.74 ± 0.26%.

To verify the validity of above correction results, another correction method is applied for comparison. Olivine composition in equilibrium with the basalt sample is calculated, using a composition-dependent Fe-Mg exchange partition coefficient ($K_{D\,Ol-Melt}^{Fe-Mg}$) (Tamura et al., 2000), and added incrementally into the basalt with the olivine composition re-iterated at each increment (0.5%) until basalt $Mg^{\#} = 72$. The method of adding olivine to evolved basaltic melts to infer their primitive magma compositions has been used in many previous studies (e.g., Cottrell & Kelley, 2011; Courtier et al., 2007; Herzberg et al., 2007; Lee et al., 2009; Putirka, 2005) but can only be applied to basalts that have undergone olivine fractionation only. In this correction, basalt samples having MgO > 8.5 wt.% (Courtier et al., 2007; Lee et al., 2009) are chosen for correction with an assumed initial melt $Fe^{3+}/\sum Fe$ of 0.15 (Cottrell & Kelley, 2011). The corrected data (with subscript 72-*AddOl*; "72-*AddOl* values") are given in Table S4.

Figure 2 compares the corrected "72-*LLD* values" and "72-*AddOl* values" for the Cenozoic basalts in eastern China. There are very tight correlations between the two sets of correction results for all the major elements (correlations for Na_2O and CaO are not shown). In addition, the data points in these diagrams are generally clustered around the 1:1 line, showing the consistency of the correction results using these two methods. Because the second correction method can only be applied to samples assumed to have undergone olivine fractionation only, we thus use the corrected "72-*LLD* values" (simplified as "72," i.e., $[SiO_2]_{72}$, $[TiO_2]_{72}$, $[Al_2O_3]_{72}$, $[FeO]_{72}$, $[MgO]_{72}$, and $[P_2O_5]_{72}$) in the following analysis and discussion.

Despite the adequacy of the fractionation correction to basalt $Mg^{\#} = 72$, uncertainties are expected for the individual sample data points, but we emphasize the first-order correlated trends defined by the data (Figure 3) in discussing the petrological significance of these basaltic melts (samples) when in equilibrium with mantle mineralogy, for example, in terms of the extent of mantle melting and pressure of melt extraction (see below).

3.2. Geochemistry of Cpx Megacrysts and *P–T* Estimation

The cpx megacrysts in these basalts have varied compositions ($Wo_{33–46}$, $En_{35–54}$, and $Fs_{9–19}$; Figure S4) with $Mg^{\#}$ = 65–85. We carried 5–16 analyses along a profile on each of the individual cpx megacrysts and found

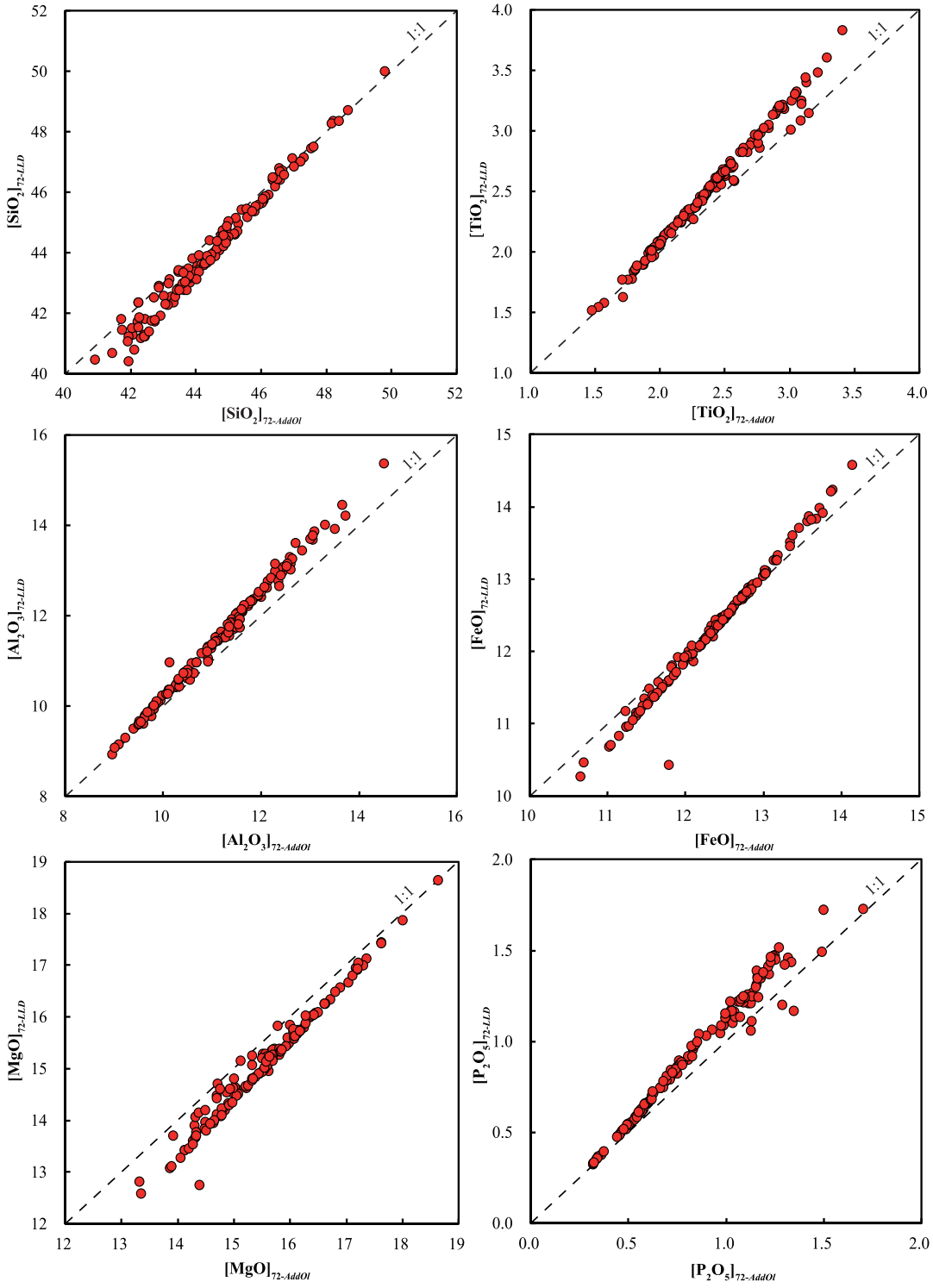

Figure 2. Comparison between the corrected "72-*LLD* values" and "72-*AddOl* values" for the Cenozoic basalts in eastern continental China. "72-*LLD* values" are the major element compositions (SiO_2, TiO_2, Al_2O_3, FeO, MgO, and P_2O_5) backtracked to $Mg^{\#} = 72$ along a set of LLDs. "72-*AddOl* values" are the major element compositions corrected to basalt $Mg^{\#} = 72$ by adding olivine. The tight correlations and large consistencies between the major element compositions corrected to $Mg^{\#} = 72$ using these two different methods prove the validity of the corrected values.

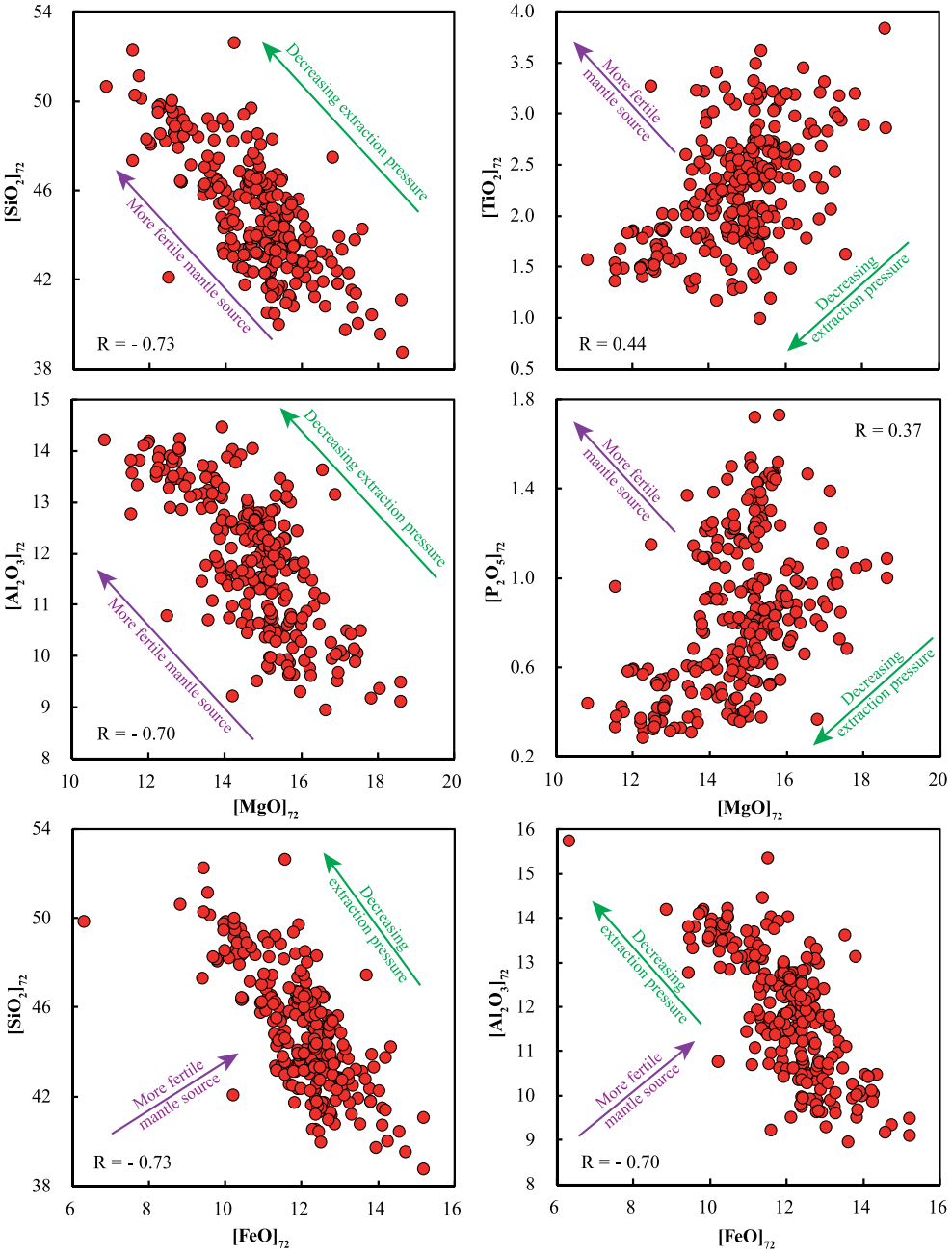

Figure 3. Correlated variations of $[MgO]_{72}$ with $[SiO_2]_{72}$, $[TiO_2]_{72}$, $[Al_2O_3]_{72}$, and $[P_2O_5]_{72}$ and correlated variations of $[FeO]_{72}$ with $[SiO_2]_{72}$ and $[Al_2O_3]_{72}$. For comparison, the compositional trends of melts derived from less to more fertile mantle compositions (the purple arrows) and from high to low pressures of melt extraction (the green arrows) are shown, respectively. These significant correlations are best explained as reflecting varying pressures of melt extraction, rather than the mantle source compositional variations.

that each megacryst is remarkably homogeneous in composition (Figure S5), indicating their crystallization in a stable environment with maintained condition and melt composition. All the cpx megacrysts have convex-upward patterns in chondrite normalized REE (rare earth element) and primitive mantle normalized trace element diagrams with relative enrichment of middle REEs (Figure S6).

There are generally two kinds of thermobarometers to calculate the equilibrium pressure (P) and temperature (T) of cpx crystallization. One is based on the P–T sensitive chemical equilibrium (i.e., T-dependent jadeite-diopside/hedenbergite exchange equilibrium and P-dependent jadeite-melt equilibrium) between

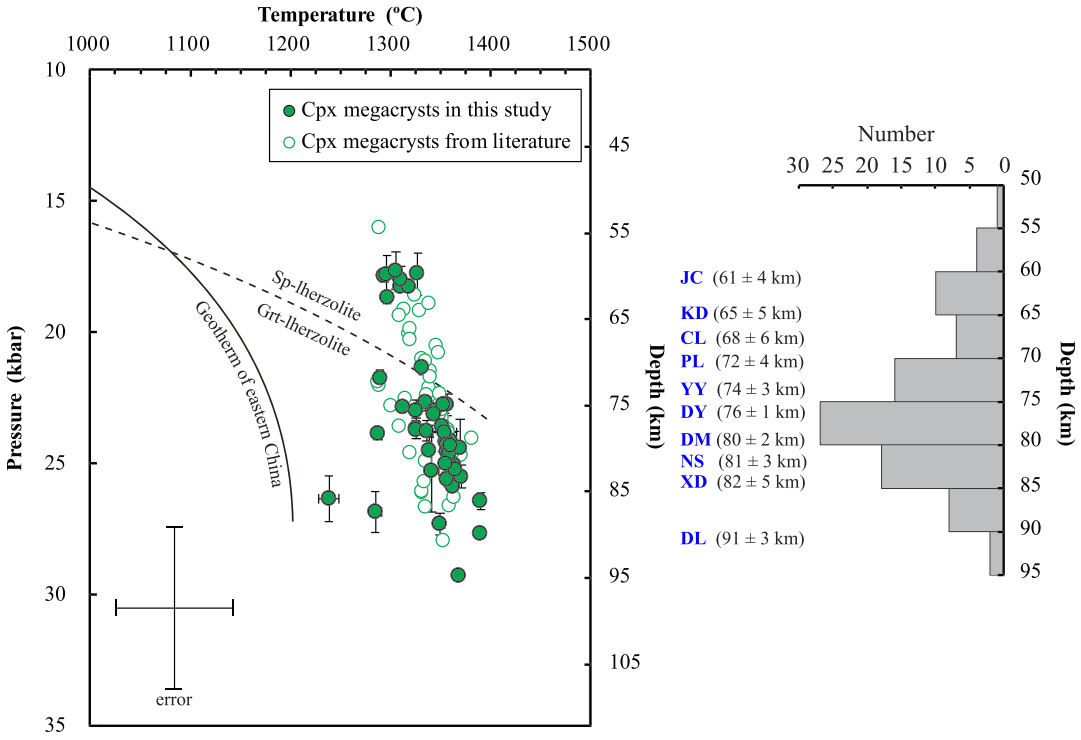

Figure 4. Calculated equilibrium temperatures and pressures of cpx megacrysts in *P*–*T* space and histogram of the calculated crystallization depths of these cpx megacrysts. The data include 47 cpx megacrysts of this study and 46 cpx megacrysts from the literature (Chen et al., 2009; Han et al., 1991; Kovács et al., 2016; Liu et al., 1992; Su et al., 2014; Wang, 2011; Xia et al., 2004; Yu et al., 2019). The cpx barometer and thermometer used are eq.32a/32d in Putirka (2008). Standard errors of *P* and *T* calculations using multiple analyses on single cpx crystals are also plotted. For comparison, the geotherm of eastern China (Menzies et al., 2007) and the transition from garnet to spinel lherzolite (Klemme & O'Neill, 2000) are also plotted. These cpx megacrysts show varied crystallization pressures of 16–29 kbar. The crystallization depths (D = 54–94 km with a peak at 75–80 km) of these cpx megacrysts are calculated using an equation of D (km) = 3.04 × P (kbar) + 5.35 created by approximating the densities of the representative crustal and mantle layers beneath eastern China (Sun et al., 2018). The location-averaged crystallization depths of cpx megacrysts from Jiucaidi (JC), Kuandian (KD), Changle (CL), Penglai (PL), Yangyuan (YY), Dayangke (DY), Damaping (DM), Nushan (NS), Xiadai (XD), and Dalinor (DL) are also listed.

cpx and host melt (cpx-melt thermobarometer; Putirka et al., 1996, 2003; Putirka, 2008). The other is based only on the cpx components (single-cpx thermobarometer; Nimis, 1995, 1999; Nimis & Taylor, 2000; Putirka, 2008). As most of the cpx megacrysts in this study are not in chemical equilibrium with their host basalts (see below), we choose to use single-cpx thermobarometer to estimate the equilibrium *P*–*T* of cpx megacryst crystallization. The cpx barometer and thermometer applied here are eq.32a and eq.32d of Putirka (2008), which are recalibrated from Nimis (1995) and Nimis and Taylor (2000), respectively, but are more precise than their original forms with systematic errors of ~±3.1 kbar and ±58 °C. The calculated *P*–*T* results are given in Table S7 and shown in Figure 4. These cpx megacrysts show variably high crystallization pressures of 16–29 kbar, corresponding to depth range of 54–94 km, using the expression D (km) = 3.04 × P (kbar) + 5.35 created by approximating the densities of the representative crustal and mantle layers beneath eastern China (Sun et al., 2018).

4. Discussion

4.1. Varying Pressures of Melt Extraction Reflected by Major Element Systematics

Peridotite melting experiments (e.g., Jaques & Green, 1980; Stolper, 1980; Walter, 1998) and modeling efforts (Niu, 1997; Niu & Batiza, 1991) showed significant control of mantle melting pressure on the major element compositions of mantle melts. With decreasing melting pressure, melt SiO_2 and Al_2O_3 increase, whereas FeO and MgO decrease. However, because of efficient and inevitable low-pressure melt-solid equilibration (Niu, 1997), the pressure signature preserved in the melt compositions largely reflects the final melting pressure (i.e., pressure of melt extraction P_f), rather than the solidus pressure (P_0) or average melting

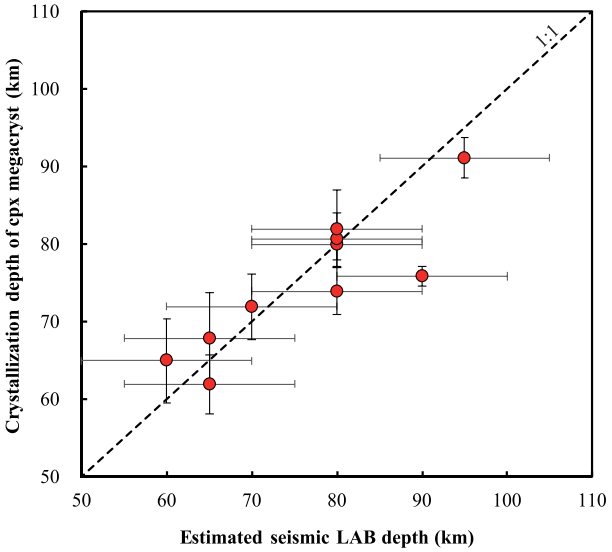

Figure 5. Comparison between the location-averaged crystallization depths of cpx megacrysts and the LAB depths beneath each sample location in eastern continental China estimated from seismic studies (Chen, 2009, 2010; Chen et al., 2008, 2009; Q. Li, Gao, et al., 2013; Y. Li, Wu, et al., 2013; Shan et al., 2016; Zheng et al., 2011). The 2SD variation ranges of the location-averaged crystallization depths of cpx megacrysts (vertical error lines) and the estimation uncertainties of the LAB depths beneath each sample locality (~±10 km; horizontal error line) are plotted.

pressure. In addition, for a polybaric decompression melting, the melt extraction pressure (P_f) is determined by the depth of the base of overlying lithosphere, which is termed "lid effect" (Humphreys & Niu, 2009; Niu et al., 2011; Niu & Green, 2018). This is proved by studies of the intraplate oceanic island basalts (OIB), which reflect a predominant control of lithosphere thickness, rather than mantle source composition, on the compositional variations of OIB. OIB extracted beneath a thick lithosphere show high-*P* signatures with low SiO_2 and Al_2O_3 and high MgO and FeO contents, whereas those extracted beneath a thin lithosphere show low-*P* signatures with high SiO_2 and Al_2O_3 and low MgO and FeO contents (Haase, 1996; Humphreys & Niu, 2009; Niu et al., 2011; Niu & Green, 2018). Furthermore, the extent of melting (F) is proportional to decompression intervals ($P_0 - P_f$). Melts extracted beneath a thick lithosphere with a low decompression interval have geochemical characteristics consistent with a low-*F* melting, showing elevated abundances of incompatible elements such as Ti and P with a strong garnet signature (high Sm/Yb). In contrast, melts extracted beneath a thin lithosphere with a longer decompression interval show high-*F* signatures with diluted Ti and P abundances and a weak garnet signature (low Sm/Yb) (Haase, 1996; Niu et al., 2011; Niu & Green, 2018).

As illustrated in Figure 3, the primitive Cenozoic basalts in eastern continental China show large compositional variations, which can be explained as reflecting varying pressures of melt extraction or varying mantle source compositions. A more fertile mantle source with higher basaltic components is characterized by high SiO_2, Al_2O_3, FeO, TiO_2, and P_2O_5 contents and low MgO content (Griffin et al., 1999, 2008; Walter, 1998). The compositional trends of melts derived from less to more fertile mantle compositions (purple arrows) and from high to low pressures of melt extraction (green arrows) are shown in Figure 3, respectively. In $[SiO_2]_{72}$-$[MgO]_{72}$ and $[Al_2O_3]_{72}$-$[MgO]_{72}$ diagrams, the compositional trends of the Cenozoic basalts in eastern continental China are consistent with both effects of mantle source fertility and melt extraction pressure. However, in the rest of these diagrams ($[TiO_2]_{72}$-$[MgO]_{72}$, $[P_2O_5]_{72}$-$[MgO]_{72}$, $[SiO_2]_{72}$-$[FeO]_{72}$, and $[Al_2O_3]_{72}$-$[FeO]_{72}$), the compositional trends are consistent with the effect of varying melt extraction pressures but orthogonal to the trend of mantle source compositional variations. Therefore, the compositional variations and correlations of primitive Cenozoic basalts in eastern China (Figure 3) can be best explained as resulting from varying pressures of melt extraction in the mantle. In terms of understood mechanisms of mantle melting and melt extraction, such varying pressures of melt extraction recorded in these basalts are most likely controlled by the varied lithosphere thickness in eastern China, specifically the depth of the lithosphere-asthenosphere boundary (LAB) as tested below.

4.2. Origin of Cpx Megacrysts in the Cenozoic Basalts of Eastern China

Cpx megacrysts in the Cenozoic basalts of eastern China have low SiO_2 (46.81–51.64 wt.%), Cr_2O_3 (0.00–0.60 wt.%), and $Mg^{\#}$ (65.2–84.3) and high Al_2O_3 (6.62–10.43 wt.%), which are different from mantle-derived Cr-rich diopsides (high SiO_2, Cr_2O_3 and $Mg^{\#}$), but similar to Al-rich augites crystallized from basaltic magmas under high pressures (Irving & Frey, 1984; Wass, 1979; Wilshire & Shervais, 1975). They show correlations of $Mg^{\#}$ with major elements and their ratios (e.g., SiO_2, TiO_2, Al_2O_3, FeO, Na_2O, and CaO/Al_2O_3) (Figure S7), suggesting their derivation from melts that had experienced variable extent of fractional crystallization. However, these cpx megacrysts are generally not in equilibrium with their host basalts (Figure S8). Most of these cpx megacrysts were crystallized from more evolved melts than their host basalts (Figure S8). Therefore, these cpx megacrysts were most likely entrained as xenocrysts by their host basalts during eruption. Nevertheless, the calculated trace element compositions and patterns of melts in equilibrium with these cpx megacrysts are essentially indistinguishable from those of the Cenozoic basalts in eastern China (Figure S9). Therefore, we suggest that the parental and host melts of these cpx megacrysts may share the similar primary melts or come from different batches of primary melts derived from similar

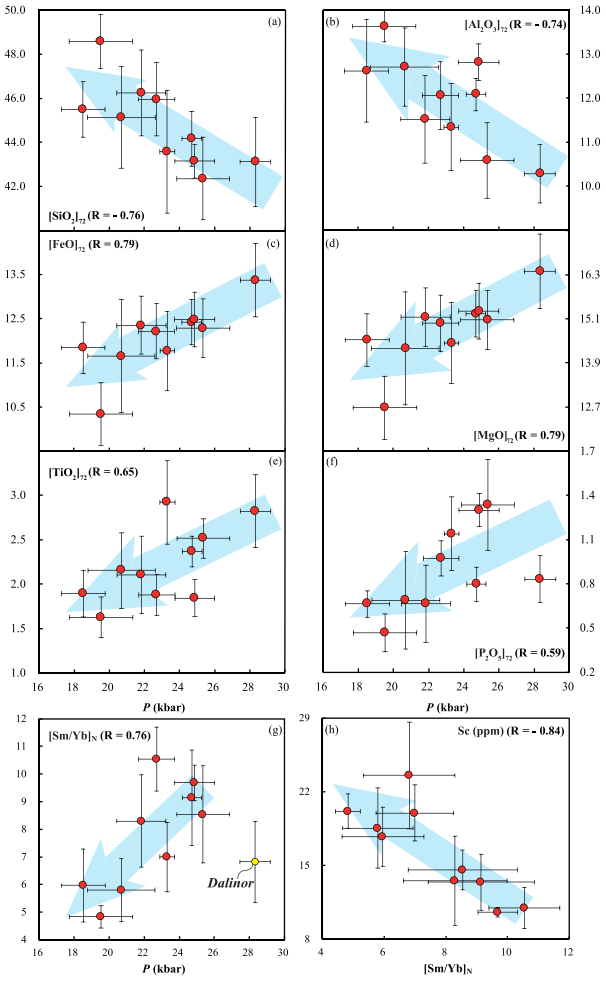

Figure 6. (a–g) Correlations of location-averaged basalt major element compositions SiO_2, TiO_2, Al_2O_3, FeO, MgO, and P_2O_5 (corrected for fractionation effect to $Mg^{\#} = 72$, e.g., $[SiO_2]_{72}$) and $[Sm/Yb]_N$ (primitive mantle normalized Sm/Yb) with location-averaged crystallization pressures of cpx megacrysts in eastern China. The basalt compositions used for correction and averaging are from 65 basalt samples analyzed in this study and 211 basalts from the literature (Basu et al., 1991; Chen et al., 2007; Chu et al., 2017; Dostal et al., 1991; Fan & Hooper, 1991; Guo et al., 2016; Guo et al., 2019; Ho et al., 2003; Huang et al., 2013; Lee et al., 2006; Liu et al., 1992, 1994; Li et al., 2016; Li et al., 2017; Liu et al., 2016; Ma & Xu, 2004; Peng et al., 1986; Qi et al., 1994; Sakuyama et al., 2013; Sun et al., 2017; Y. Wang, Zhao, et al., 2011; Xu et al., 2012; Yang et al., 2012; Zou et al., 2000). The crystallization pressures of cpx megacrysts used for averaging are calculated from cpx compositions analyzed in this study and those compiled from the literature (Chen et al., 2009; Han et al., 1991; Kovács et al., 2016; Liu et al., 1992; Su et al., 2014; Wang, 2011; Xia et al., 2004; Yu et al., 2019). Each data point represents average cpx crystallization pressure (*X* axis) and average basalt composition (*Y* axis) from a given location; the error bars represent one standard derivation from the mean. The variation of crystallization pressures of cpx megacrysts represents the variation of lithosphere thickness beneath each sample locality in eastern continental China (Figure 1; see text for details). The averaged data points define trends that are consistent with decreasing pressure and increasing extent of melting from beneath thick lithosphere (high $[MgO]_{72}$, $[FeO]_{72}$, $[TiO_2]_{72}$, $[P_2O_5]_{72}$, and $[Sm/Yb]_N$ and low $[SiO_2]_{72}$, and $[Al_2O_3]_{72}$) to beneath thin lithosphere (low $[MgO]_{72}$, $[FeO]_{72}$, $[TiO_2]_{72}$, $[P_2O_5]_{72}$, and $[Sm/Yb]_N$ and high $[SiO_2]_{72}$ and $[Al_2O_3]_{72}$), demonstrating significant control of lithosphere thickness on the compositional variation of continental intraplate basalts. Data point of Dalinor in the $[Sm/Yb]_N$ versus *P* diagram is off the trend, which may indicate the average calculated pressure higher than the LAB depth beneath this region. (h) Correlation between location-averaged basalt $[Sm/Yb]_N$ and Sc contents to show the "garnet" effect on the basalt trace element compositions. As Sc is highly compatible in garnet, residence of garnet in the mantle source region beneath thick lithosphere can result in both low Sc contents and high $[Sm/Yb]_N$ in the erupted melt. In contrast, melts derived from beneath thin lithosphere have high Sc contents and low $[Sm/Yb]_N$.

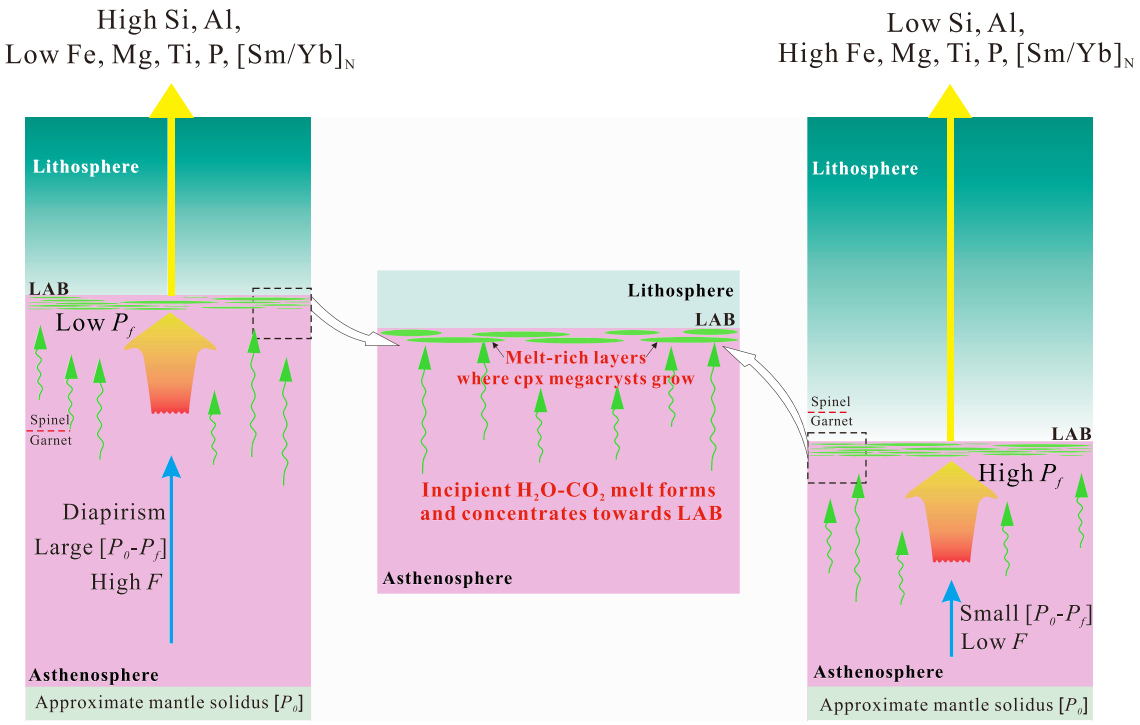

Figure 7. Schematic illustration of the lithospheric thickness control on the compositional variation of intraplate basalts beneath eastern continental China. The adiabatically upwelling mantle reaches the solidus and begins to melt at P_0. The base of the lithosphere constrains the final depth of the melting (P_f). The vertical range of decompression ($P_0 - P_f$) is proportional to the extent of melting (F). The melts erupted on thick lithosphere show signatures of high pressure and low extent of melting (i.e., low Si and Al and high Fe, Mg, P, and Ti), whereas those erupted on thin lithosphere show the signatures of low melting pressure and high extent of melting (i.e., high Si and Al and low Fe, Mg, P, and Ti). Furthermore, melting beneath thick lithosphere in the garnet facies can impart strong "garnet signature" in the derived melt with high $[Sm/Yb]_N$, whereas the intensity of "garnet signature" can be diluted by increasing extent of melting beneath thin lithosphere, with the melt having low $[Sm/Yb]_N$. The green layer beneath the LAB indicates the presence of a melt-rich layer (supplied by the rising incipient melt denoted by the green arrowed wavy lines). Localized melt layers embedded in the meltless asthenosphere close beneath the LAB can act as stable "magma reservoirs" with closed-system crystallization to form evolved melts and cpx megacrysts without being in equilibrium with surrounding mantle.

sources and under similar conditions. This is also favored by the similarly depleted Sr-Nd isotope compositions between cpx megacrysts and their host basalts shown in previous studies (He et al., 2013; Liu et al., 1992; Yu et al., 2019).

The characteristics of vitreous appearance and conchoidal fracture with poor cleavage of these cpx megacrysts are consistent with cpx megacrysts found in alkali basalts in south Australia and Scotland which were suggested to have a high-pressure origin (Chapman, 1976; Irving, 1974). Calculations using the pyroxene geobarometer confirm the high-pressure signature (16–29 kbar) of these cpx megacrysts in eastern China. Similar cpx megacrysts with a high-pressure origin have also been reported in the Cenozoic alkali basalts from the Chukchi Peninsula in the far east Asia (Akinin et al., 2005). It should be noted that the crystallization depth range (54–94 km) of the cpx megacrysts in eastern China is similar to the depth range of present-day lithosphere-asthenosphere boundary (LAB) beneath eastern China (~60–100 km; e.g., An & Shi, 2006; Chen et al., 2008; Chen, 2009), and the average crystallization depth of cpx megacrysts from a given location (Figure 4) is close to the estimated seismic LAB depth beneath this region, despite of the large uncertainties of these estimations (Figure 5). Therefore, we conclude that these cpx megacrysts were most likely crystallized under conditions close to the LAB and then captured as xenocrysts by their rapid-ascending host basalts.

4.3. Lithospheric Thickness Control on the Compositional Variation of Continental Intraplate Basalts

Although the LAB depth beneath a given location in eastern continental China can be estimated from seismic studies (Figure 5), such estimation is rough because of the low resolutions (~10 km) of seismic models and because LAB beneath this region is in fact a gradient zone 10–20 km wide rather than an ideal sharp

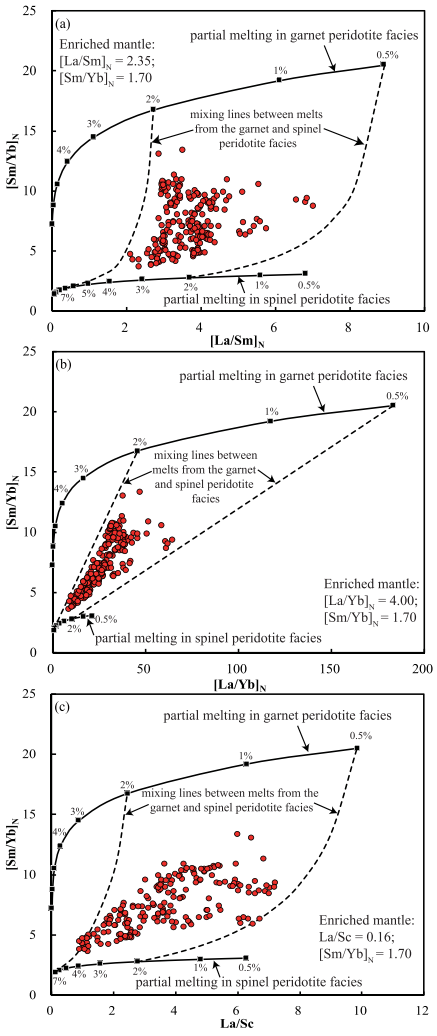

Figure 8. (a) $[Sm/Yb]_N$ versus $[La/Sm]_N$, (b) $[Sm/Yb]_N$ versus $[La/Yb]_N$, and (c) $[Sm/Yb]_N$ versus La/Sc for the Cenozoic basalts in eastern China. The solid curves show non-modal fractional melting models in the garnet and spinel peridotite facies, respectively. The dashed curves show mixing trends between a 0.5% melt from the garnet peridotite facies and a 2% melt from the spinel peridotite facies and between a 2% melt from the garnet peridotite facies and a 7% melt from the spinel peridotite facies, respectively. The source and melt mineral modes in garnet and spinel peridotite facies are from the compilation in Johnson (1998). Partition coefficients are from the compilation in Niu et al. (1996). The source mantle of the Cenozoic basalts in eastern China was suggested to have fertile major element compositions similar to the primitive mantle (PM) (e.g., Wu et al., 2006; Xu et al., 2000) but is more enriched in progressively more incompatible elements, which is consistent with a low-degree melt metasomatism in the low velocity zone (LVZ) prior to the major melting event (e.g., Guo et al., 2016; Niu, 2005; Sun et al., 2017). Therefore, the enriched source mantle of the Cenozoic basalts in eastern China is estimated to be a mixture of PM with 5% of a low-degree (0.5%) melt from the PM. This source mantle composition can well explain the high $[La/Sm]_N$ (an indicator of the source enrichment) of these basalts. The PM composition is from McDonough and Sun (1995). This partial melting modeling shows that these basalts represent mixing between small melt fractions from the garnet peridotite facies with high $[Sm/Yb]_N$, $[La/Yb]_N$, and La/Sc ratios and relatively larger melt fractions from spinel peridotite facies with lower $[Sm/Yb]_N$, $[La/Yb]_N$, and La/Sc ratios.

boundary (e.g., Chen, 2009; Chen et al., 2008). In addition, different seismic studies tend to give varied LAB depths beneath a given location. Hence, estimation of the LAB depth beneath a given location is to some extent artificial. Therefore, unlike the oceanic lithosphere whose thickness (L) can be well estimated from its age (t) by the half-space cooling model (HSM) $L \propto t^{1/2}$ (e.g., Parsons & McKenzie, 1978; Sclater & Francheteau, 1970), it is difficult to constrain the continental lithosphere thickness and evaluate its compositional control on the within-continental basalts. However, in the case of the Cenozoic basalts in eastern continental China, if their pressure signatures revealed by the compositional variations (Figure 3) are indeed controlled by the varying lithosphere thickness, and if the cpx megacrysts included in these basalts are indeed formed under conditions close to the LAB (see above), we should expect correlated variations of basalt compositions with the calculated crystallization pressures of cpx megacrysts.

Indeed, Figure 6 confirms this prediction. Figures 6a–6f show correlated variations of the location-averaged basalt compositions with the location-averaged crystallization pressures of cpx megacrysts (see data in Table S8). Basalts containing cpx megacrysts with high crystallization pressures derived from beneath thick lithosphere have compositions of low $[SiO_2]_{72}$ and $[Al_2O_3]_{72}$ and high $[FeO]_{72}$, $[MgO]_{72}$, $[TiO_2]_{72}$, and $[P_2O_5]_{72}$ because of low extent (F) of melting and high pressure (deep) melt extraction (P_f), whereas basalts containing cpx megacrysts with low crystallization pressures derived from beneath thin lithosphere exhibit the reverse, that is, high $[SiO_2]_{72}$ and $[Al_2O_3]_{72}$ and low $[FeO]_{72}$, $[MgO]_{72}$, $[TiO_2]_{72}$, and $[P_2O_5]_{72}$ (Humphreys & Niu, 2009; Niu et al., 2011) (Figure 7).

Furthermore, melting beneath thick lithosphere in the garnet peridotite facies can impart the strong "garnet signature" in the resulting melt with high $[Sm/Yb]_N$ (primitive mantle normalized Sm/Yb), whereas the intensity of the "garnet signature" is diluted by the continued decompression melting beneath thin lithosphere, with the resulting melt having low $[Sm/Yb]_N$ (Figure 7; Humphreys & Niu, 2009; Niu et al., 2011). The positive correlation between the location-averaged basalt $[Sm/Yb]_N$ and crystallization pressures of cpx megacrysts confirms this reasoning and understanding (Figure 6g).

Such "garnet" effect on the basalt trace element compositions can be demonstrated and substantiated by the negative correlation between basalt Sc content and $[Sm/Yb]_N$ (Figure 6h) because Sc is highly compatible in garnet as are heavy REEs like Yb, hence the positive Sc-Yb correlation and negative Sc-$[Sm/Yb]_N$. Partial melting modeling in Figure 8 further confirms the above explanation that the Cenozoic basalts in eastern China were derived from partial melts from the garnet peridotite facies which were then diluted by melts from the spinel peridotite facies by variable extents. Melts derived from beneath a thick lithosphere mainly in the garnet peridotite facies experience less extent of dilution and show high $[Sm/Yb]_N$, $[La/Yb]_N$, and La/Sc ratios, whereas melts derived from beneath a thin lithosphere experience higher extent of partial melting in the spinel peridotite facies and have low $[Sm/Yb]_N$, $[La/Yb]_N$, and La/Sc ratios. Such modeling is only semiquantitative as the composition of the enriched mantle source beneath eastern China is difficult to constrain. However, modeling involved $[La/Sm]_N$ can place some convincing

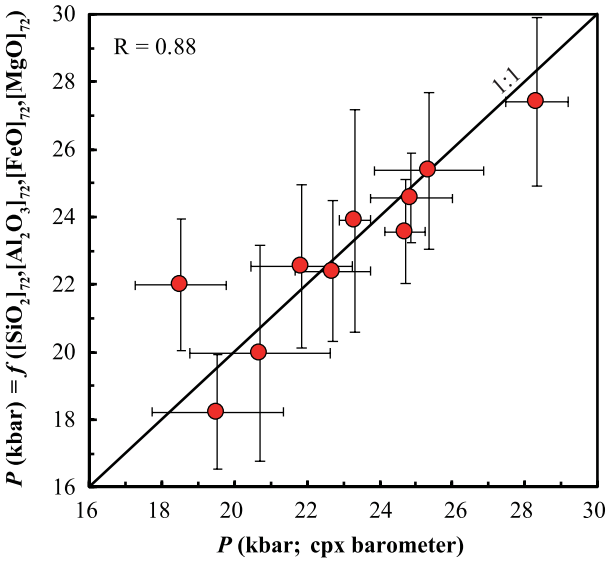

Figure 9. A multivariate regression expresses the lithosphere thickness (shown by the crystallization pressures of cpx megacrysts) in terms of several pressure-sensitive parameters in Figure 6 ($[SiO_2]_{72}$, $[Al_2O_3]_{72}$, $[MgO]_{72}$, and $[FeO]_{72}$), which emphasizes that basalts record faithfully only the final depth of melting or melt equilibration, instead of initial nor mean pressure of melting.

constraints on the mantle source composition of these basalts because $[La/Sm]_N$ is more sensitive to the source enrichment than mantle peridotite facies (garnet/spinel) (Figure 8a). In conclusion, the correlations in Figure 6 demonstrate the significant control of lithosphere thickness on both major and trace element compositions of continental intraplate basalts and confirm a high-pressure origin of cpx megacrysts at sites close to the LAB.

The various *P*-indicating petrological parameters ($[SiO_2]_{72}$, $[Al_2O_3]_{72}$, $[MgO]_{72}$, and $[FeO]_{72}$) in Figure 6 can be combined into a single *P*-parameter, expressed in terms of lithosphere thickness (shown by the crystallization pressures of cpx megacrysts) using a polynomial regression ($R = 0.88$) (Figure 9). It should be noted that such basalt-based *P* values represent the final melt extraction pressures, determined by the thickness of the lithospheric lid, rather than any melting pressure (e.g., initial or average melting pressures) deeper than the LAB, because of the extremely efficient melt-solid equilibration under sublithospheric mantle conditions (Niu, 1997; Niu et al., 2011). Therefore, application of basalt-based thermobarometers to infer the initial pressure and temperature of mantle melting is problematic and misleading (Niu, 2016; Niu et al., 2011) because basalts do not record such information.

4.4. Implications on the Crystallization Sites of Cpx Megacrysts

The above discussions on the origin of cpx megacrysts have confirmed their high crystallization pressures close to the depths of LAB. However, one important but often overlooked problem is that why these cpx megacrysts crystallized close to the LAB are so evolved instead of being in equilibrium with primitive mantle melts with $Mg^{\#} \geq 72$ (Figure S8). The highly evolved nature of these cpx megacrysts indicates the presence of variably evolved parental melts close to the LAB. One possible site where these evolved melts exist may be the magma chambers at the base of continental lithospheric mantle. However, it is not clear how these magma chambers were formed under such high pressures in the refractory lithospheric mantle resistant to melt erosion and why these magma chambers must necessarily exist close to the LAB. In Irving's "flow crystallization" model, crystallization can take place along the walls of magma conduits from a flowing melt (Irving, 1974, 1980). This is possible and likely but requires a conduit with sufficient width, a slow magma flowing rate, continued magma supply from the deep mantle, and long-term uniform parental magma composition in order to generate large compositionally homogeneous cpx megacrysts. However, the widespread appearance of mantle xenoliths in the Cenozoic basalts in eastern China implies a rapid magma ascending rate, and it is difficult to keep long-term uniform and evolved compositions for melts flowing in the magma conduits. Therefore, magma chambers and magma conduits at the base of continental lithospheric mantle may not be reasonable sites for the growth of cpx megacrysts.

The upper mantle seismic structure beneath eastern China has been detected to resemble that of the oceanic upper mantle with a seismic low velocity zone (LVZ) beneath the lithosphere (Ekström & Dziewonski, 1998), which requires the presence of a melt rich layer close beneath the LAB (Figure 7; e.g., Kawakatsu et al., 2009; Naif et al., 2013; Niu, 2008; Niu & O'Hara, 2009; Niu et al., 2011; Niu & Green, 2018; Schmerr, 2012; Tharimena et al., 2017). Such localized melt layers (or lenses) can act as stable "magma reservoirs" with closed-system crystallization (Figure 7) to form evolved melts parental to these compositionally evolved and uniform cpx megacrysts without dynamic reaction with the surrounding mantle. Therefore, these cpx megacrysts were most likely crystallized in closed and stable melt layers close beneath the LAB, and their crystallization depths (pressures) can thus be used as effective proxies for the lithosphere thickness. Such a "stable and closed system magma reservoir" is expected to be destructed or demolished by the next pulses of melt aggregation, transport, and eruption, with previously crystallized cpx megacrysts captured as xenocrysts by the replenished and ascending melts. It is important to note that cpx megacrysts transporting melt may undergo further crystallization during ascent because of decompression-induced volatile exsolution, which can raise the liquidus temperature, leading to the

variably evolved host melt composition (Sun et al., 2018). This understanding offers new insights into mantle melting and melt aggregation processes for continental basaltic magmatism.

5. Conclusions

We test the hypothesis that lithospheric thickness controls the compositional variation of continental intraplate basalts by studying the Cenozoic alkali basalts and the contained clinopyroxene megacrysts from 10 localities throughout eastern continental China. These clinopyroxene megacrysts were formed at sites close to the base of the lithospheric mantle, and their equilibrium pressures (depths) are thus ideal proxies for the lithosphere thickness at the time of eruptions. Melts erupted on thick lithosphere have geochemical characteristics of lower extent of melting (e.g., higher $[TiO_2]_{72}$, $[P_2O_5]_{72}$, and $[Sm/Yb]_N$) and higher pressure of melt extraction (e.g., lower $[SiO_2]_{72}$, $[Al_2O_3]_{72}$, and Sc; higher $[MgO]_{72}$, $[FeO]_{72}$, and $[Sm/Yb]_N$), whereas basalts erupted on thin lithosphere have the signatures of higher extent of melting (e.g., lower $[TiO_2]_{72}$, $[P_2O_5]_{72}$, and $[Sm/Yb]_N$) and lower pressure of melt extraction (e.g., higher $[SiO_2]_{72}$, $[Al_2O_3]_{72}$, and Sc; lower $[MgO]_{72}$, $[FeO]_{72}$, and $[Sm/Yb]_N$). Therefore, the basalt compositions reflect the final pressure of melting or melt equilibrium, determined by the thickness of lithospheric lid, rather than pressure conditions deeper than the LAB, because of efficient melt-solid equilibration during the process of melt extraction. Importantly, a melt rich layer close beneath the LAB required to explain the seafloor basalt petrogenesis also exists beneath continents. Such a melt layer forms a "stable and closed-system magma reservoir" to crystallize compositionally uniform cpx megacrysts. Such a "magma reservoir" will be destructed or demolished by the next pulses of melt aggregation, transport and eruption. Hence, both the cpx megacrysts and the host basalts record different aspects of the same control, that is, the lid effect, on continental basaltic magmatism.

Acknowledgments
We thank Dr. Emily J. Chin, Dr. Ian Campbell, two anonymous reviewers, Editor Stephen Parman, and the associate editor for their useful comments on earlier versions of this paper. This work was supported by the NSFC-Shandong Joint Fund for Marine Science Research Centers (U1606401), the National Natural Science Foundation of China (NSFC Grants 41630968, 41776067, 41130314, 91014003), Chinese Academy of Sciences (Innovation Grant Y42217101L), and grants from Qingdao National Laboratory for Marine Science and Technology (2015ASKJ03) and 111 Project (B18048). The data used in this paper are provided in https://doi.org/10.6084/m9.figshare.11473059.v1.

References

Akinin, V. V., Sobolev, A. V., Ntaflos, T., & Richter, W. (2005). Clinopyroxene megacrysts from Enmelen melanephelinitic volcanoes (Chukchi Peninsula, Russia): Application to composition and evolution of mantle melts. *Contributions to Mineralogy and Petrology*, *150*(1), 85–101.

An, M., & Shi, Y. (2006). Lithospheric thickness of the Chinese continent. *Physics of the Earth and Planetary Interiors*, *159*(3), 257–266.

Basu, A. R., Wang, J., Huang, W., Xie, G., & Tatsumoto, M. (1991). Major element, REE, and Pb, Nd and Sr isotopic geochemistry of Cenozoic volcanic rocks of eastern China: Implications for their origin from suboceanic-type mantle reservoirs. *Earth and Planetary Science Letters*, *105*(1), 149–169.

Chapman, N. A. (1976). Inclusions and megacrysts from undersaturated tuffs and basanites, East Fife, Scotland. *Journal of Petrology*, *17*(4), 472–498.

Chen, D., Xia, Q., & Zhi, X. (1997). Geochemistry of clinopyroxene megacrysts from Nushan, Anhui (in Chinese with English abstract). *Acta Mineralogica Sinica*, *17*(3), 260–269.

Chen, H., Xia, Q.-K., Ingrin, J., Deloule, E., & Bi, Y. (2017). Heterogeneous source components of intraplate basalts from NE China induced by the ongoing Pacific slab subduction. *Earth and Planetary Science Letters*, *459*, 208–220.

Chen, L. (2009). Lithospheric structure variations between the eastern and central North China Craton from S- and P-receiver function migration. *Physics of the Earth and Planetary Interiors*, *173*(3), 216–227.

Chen, S., Wang, X., Niu, Y., Sun, P., Duan, M., Xiao, Y., et al. (2017). And cost-effective methods for precise analysis of trace element abundances in geological materials with ICP-MS. *Science Bulletin*, *62*(4), 277–289.

Chen, L. (2010). Concordant structural variations from the surface to the base of the upper mantle in the North China Craton and its tectonic implications. *Lithos*, *120*(1), 96–115.

Chen, L., Tao, W., Zhao, L., & Zheng, T. (2008). Distinct lateral variation of lithospheric thickness in the Northeastern North China Craton. *Earth and Planetary Science Letters*, *267*(1–2), 56–68.

Chen, L., Zheng, T., & Xu, W. (2006). A thinned lithospheric image of the Tanlu Fault Zone, eastern China: Constructed from wave equation based receiver function migration. *Journal of Geophysical Research*, *111*, B09312. https://doi.org/10.1029/2005JB003974

Chen, X., Chen, L., & Xu, X. (2009). Study on the genesis of clinopyroxene megacrysts in the Cenozoic alkali basalts at Changle, Shandong Province (in Chinese with English abstract). *Acta Petrologica Sinica*, *25*(5), 1105–1116.

Chen, Y., Zhang, Y., Graham, D., Su, S., & Deng, J. (2007). Geochemistry of Cenozoic basalts and mantle xenoliths in Northeast China. *Lithos*, *96*(1), 108–126.

Chin, E. J. (2018). Deep crustal cumulates reflect patterns of continental rift volcanism beneath Tanzania. *Contributions to Mineralogy and Petrology*, *173*(10), 85.

Chu, Z., Yan, Y., Zeng, G., Tian, W., Li, C., Yang, Y., & Guo, J. (2017). Petrogenesis of Cenozoic basalts in Central-Eastern China: Constraints from Re–Os and PGE geochemistry. *Lithos*, *278-281*, 72–83.

Cottrell, E., & Kelley, K. A. (2011). The oxidation state of Fe in MORB glasses and the oxygen fugacity of the upper mantle. *Earth and Planetary Science Letters*, *305*(3), 270–282.

Courtier, A. M., Jackson, M. G., Lawrence, J. F., Wang, Z., Lee, C. T. A., Halama, R., et al. (2007). Correlation of seismic and petrologic thermometers suggests deep thermal anomalies beneath hotspots. *Earth and Planetary Science Letters*, *264*(1-2), 308–316. https://doi.org/10.1016/j.epsl.2007.10.003

Davies, D. R., Rawlinson, N., Iaffaldano, G., & Campbell, I. H. (2015). Lithospheric controls on magma composition along Earth's longest continental hotspot track. *Nature*, *525*, 511–514.

Dobosi, G., & Jenner, G. (1999). Petrologic implications of trace element variation in clinopyroxene megacrysts from the Nograd volcanic province, north Hungary: A study by laser ablation microprobe-inductively coupled plasma-mass spectrometry. *Lithos*, *46*(4), 731–749.
Dostal, J., Zhi, X., Muehlenbachs, K., Dupuy, C., & Zhai, M. (1991). Geochemistry of Cenozoic alkali basaltic lavas from Shandong Province, eastern China. *Geochemical Journal*, *25*(1), 1–16.
Ekström, G., & Dziewonski, A. M. (1998). The unique anisotropy of the Pacific upper mantle. *Nature*, *394*, 168–172.
Fan, Q., & Hooper, P. R. (1991). The Cenozoic basaltic rocks of eastern China: Petrology and chemical composition. *Journal of Petrology*, *32*(4), 765–810.
Flower, M. F., Zhang, M., Chen, C.-Y., Tu, K., & Xie, G. (1992). Magmatism in the south China basin: 2. Post-spreading Quaternary basalts from Hainan Island, south China. *Chemical Geology*, *97*(1), 65–87.
Gao, S., Rudnick, R. L., Yuan, H.-L., Liu, X.-M., Liu, Y.-S., Xu, W.-L., et al. (2004). Recycling lower continental crust in the North China Craton. *Nature*, *432*(7019), 892–897. https://doi.org/10.1038/nature03162
Green, D. H., & Ringwood, A. E. (1967). The genesis of basaltic magmas. *Contributions to Mineralogy and Petrology*, *15*(2), 103–190.
Griffin, W., Andi, Z., O'reilly, S., & Ryan, C. (1998). Phanerozoic evolution of the lithosphere beneath the Sino-Korean craton. In M. F. J. Flower, S.-L. Chung, C.-H. Lo, & T.-Y. Lee (Eds.), *Mantle dynamics and plate interactions in East Asia* (Vol. 27, pp. 107–126). Washington, DC: American Geophysical Union.
Griffin, W., O'Reilly, S., & Ryan, C. (1999). The composition and origin of sub-continental lithospheric mantle. In Y. Fei, C. M. Bertka, & B. O. Mysen (Eds.), *Mantle petrology: Field observations and high pressure experimentation: A tribute to Francis R. (Joe) Boyd* (pp. 13–45). Houston: The Geochemical Society, Special Publication, Geochemical Society.
Griffin, W. L., O'Reilly, S. Y., Afonso, J. C., & Begg, G. C. (2008). The composition and evolution of lithospheric mantle: A re-evaluation and its tectonic implications. *Journal of Petrology*, *50*(7), 1185–1204.
Guo, P., Niu, Y., Sun, P., Gong, H., & Wang, X. (2019). Lithosphere thickness controls continental basalt compositions: An illustration using Cenozoic basalts from eastern China. *Geology*, *48*(2), 128–133.
Guo, P., Niu, Y., Sun, P., Ye, L., Liu, J., Zhang, Y., et al. (2016). The origin of Cenozoic basalts from Central Inner Mongolia, East China: The consequence of recent mantle metasomatism genetically associated with seismically observed paleo-Pacific slab in the mantle transition zone. *Lithos*, *240-243*, 104–118.
Haase, K. M. (1996). The relationship between the age of the lithosphere and the composition of oceanic magmas: Constraints on partial melting, mantle sources and the thermal structure of the plates. *Earth and Planetary Science Letters*, *144*(1), 75–92.
Han, Z., Sheng, X., & Zhao, G. (1991). Mineral Chemistry of megacrysts and spinel lherzolite xenoliths in Cenozoic era basalts from Ponglai. *Journal of Ocean University of Qingdao*, *21*(1), 91–100. [in Chinese with English abstract]
He, D., Liu, Y., Tong, X., Zong, K., Hu, Z., & Gao, S. (2013). Multiple exsolutions in a rare clinopyroxene megacryst from the Hannuoba basalt, North China: Implications for subducted slab-related crustal thickening and recycling. *Lithos*, *177*, 136–147.
Helz, R. T. (1987). Differentiation behavior of Kilauea Iki lava lake, Kilauea Volcano, Hawaii: An overview of past and current work. In B. O. Mysen (Ed.), *Magmatic processes: physicochemical principles* (pp. 241–258). University Park, PA: The Geochemical Society, Special Publication No. 1
Herzberg, C., Asimow, P. D., Arndt, N., Niu, Y., Lesher, C., Fitton, J., et al. (2007). Temperatures in ambient mantle and plumes: Constraints from basalts, picrites, and komatiites. *Geochemistry, Geophysics, Geosystems*, *8*, Q02206. https://doi.org/10.1029/2006GC001390
Ho, K.-S., Chen, J.-C., Lo, C.-H., & Zhao, H.-L. (2003). ^{40}Ar–^{39}Ar dating and geochemical characteristics of late Cenozoic basaltic rocks from the Zhejiang–Fujian region, SE China: Eruption ages, magma evolution and petrogenesis. *Chemical Geology*, *197*(1), 287–318.
Huang, X.-L., Niu, Y., Xu, Y.-G., Ma, J.-L., Qiu, H.-N., & Zhong, J.-W. (2013). Geochronology and geochemistry of Cenozoic basalts from eastern Guangdong, SE China: Constraints on the lithosphere evolution beneath the northern margin of the South China Sea. *Contributions to Mineralogy and Petrology*, *165*(3), 437–455.
Humphreys, E. R., & Niu, Y. (2009). On the composition of ocean island basalts (OIB): The effects of lithospheric thickness variation and mantle metasomatism. *Lithos*, *112*(1), 118–136.
Irving, A. J. (1974). Megacrysts from the newer basalts and other basaltic rocks of southeastern Australia. *Geological Society of America Bulletin*, *85*, 1503–1514.
Irving, A. J. (1980). Petrology and geochemistry of composite ultramafic xenoliths in alkalic basalts and implications for magmatic processes within the mantle. *American Journal of Science*, *280*(2), 389–426.
Irving, A. J., & Frey, F. A. (1984). Trace element abundances in megacrysts and their host basalts: Constraints on partition coefficients and megacryst genesis. *Geochimica et Cosmochimica Acta*, *48*(6), 1201–1221.
Jaques, A., & Green, D. (1980). Anhydrous melting of peridotite at 0–15 kb pressure and the genesis of tholeiitic basalts. *Contributions to Mineralogy and Petrology*, *73*(3), 287–310.
Johnson, K. T. (1998). Experimental determination of partition coefficients for rare earth and high-field-strength elements between clinopyroxene, garnet, and basaltic melt at high pressures. *Contributions to Mineralogy and Petrology*, *133*(1–2), 60–68.
Kawakatsu, H., Kumar, P., Takei, Y., Shinohara, M., Kanazawa, T., Araki, E., & Suyehiro, K. (2009). Seismic evidence for sharp lithosphere-asthenosphere boundaries of oceanic plates. *Science*, *324*(5926), 499–502. https://doi.org/10.1126/science.1169499
Klemme, S., & O'Neill, H. S. (2000). The near-solidus transition from garnet lherzolite to spinel lherzolite. *Contributions to Mineralogy and Petrology*, *138*(3), 237–248.
Kovács, I., Demény, A., Czuppon, G., Lécuyer, C., Fourel, F., Xia, Q. K., et al. (2016). Water concentrations and hydrogen isotope compositions of alkaline basalt-hosted clinopyroxene megacrysts and amphibole clinopyroxenites: The role of structural hydroxyl groups and molecular water. *Contributions to Mineralogy and Petrology*, *171*(5), 38. https://doi.org/10.1007/s00410-016-1241-0
Lee, C.-T., Luffi, P., Plank, T., Dalton, H., & Leeman, W. P. (2009). Constraints on the depths and temperatures of basaltic magma generation on Earth and other terrestrial planets using new thermobarometers for mafic magmas. *Earth and Planetary Science Letters*, *279*(1), 20–33. https://doi.org/10.1016/j.epsl.2008.12.020 Lee, Y.-T., Chen, J.-C., Shih, J.-Y., Juang, W.-S., Yang, H.-J., Huang, S.-W., & Lin, M.-L. (2006). Geochemistry of Cenozoic basaltic rocks from Shandong Province and its implication for mantle process in North China. *Geochemical Journal*, *40*(6), 579–596.
Li, N., Gong, L., Zhao, Y., Fan, Q., Wang, J., & Zhang, C. (2017). Characteristics of volcanic geomorphology in Dalinor volcanic swarm and petrologic features of the volcanic rocks, Inner Mongolia (in Chinese with English abstract). *Acta Petrologica Sinica*, *33*(1), 137–147.
Li, Q., Gao, R., Wu, F. T., Guan, Y., Ye, Z., Liu, Q., et al. (2013). Seismic structure in the southeastern China using teleseismic receiver functions. *Tectonophysics*, *606*, 24–35.

Li, Y., Wu, Q., Pan, J., Zhang, F., & Yu, D. (2013). An upper-mantle S-wave velocity model for East Asia from Rayleigh wave tomography. *Earth and Planetary Science Letters*, *377-378*, 367–377.
Li, Y.-Q., Ma, C.-Q., & Robinson, P. T. (2016). Petrology and geochemistry of Cenozoic intra-plate basalts in east-central China: Constraints on recycling of an oceanic slab in the source region. *Lithos*, *262*, 27–43.
Liu, C.-Q., Masuda, A., & Xie, G.-H. (1992). Isotope and trace-element geochemistry of alkali basalts and associated megacrysts from the Huangyishan volcano, Kuandian, Liaoning, NE China. *Chemical Geology*, *97*(3), 219–231.
Liu, C.-Q., Masuda, A., & Xie, G.-H. (1994). Major- and trace-element compositions of Cenozoic basalts in eastern China: Petrogenesis and mantle source. *Chemical Geology*, *114*(1), 19–42.
Liu, S.-C., Xia, Q.-K., Choi, S. H., Deloule, E., Li, P., & Liu, J. (2016). Continuous supply of recycled Pacific oceanic materials in the source of Cenozoic basalts in SE China: The Zhejiang case. *Contributions to Mineralogy and Petrology*, *171*(12), 100.
Liu, Y.-D., & Ying, J.-F. (2019). Origin of clinopyroxene megacrysts in volcanic rocks from the North China Craton: A comparison study with megacrysts worldwide. *International Geology Review*, *1-17*. https://doi.org/10.1080/00206814.2019.1663766
Ma, J., & Xu, Y. (2004). Petrology and geochemistry of the Cenozoic basalts from Yangyuan of Hebei Province and Datong of Shanxi Province: Implications for the deep process in the western North China Craton (in Chinese with English abstract). *Geochimica*, *33*(1), 75–88.
McDonough, W. F., & Sun, S. S. (1995). The composition of the Earth. *Chemical Geology*, *120*(3), 223–253.
Menzies, M., Xu, Y., Zhang, H., & Fan, W. (2007). Integration of geology, geophysics and geochemistry: A key to understanding the North China Craton. *Lithos*, *96*(1), 1–21.
Menzies, M. A., Fan, W., & Zhang, M. (1993). Palaeozoic and Cenozoic lithoprobes and the loss of >120 km of Archaean lithosphere, Sino-Korean craton, China. *Geological Society, London, Special Publications*, *76*(1), 71.
Naif, S., Key, K., Constable, S., & Evans, R. L. (2013). Melt-rich channel observed at the lithosphere–asthenosphere boundary. *Nature*, *495*(7441), 356–359. https://doi.org/10.1038/nature11939
Nimis, P. (1995). A clinopyroxene geobarometer for basaltic systems based on crystal-structure modeling. *Contributions to Mineralogy and Petrology*, *121*(2), 115–125.
Nimis, P. (1999). Clinopyroxene geobarometry of magmatic rocks. Part 2. Structural geobarometers for basic to acid, tholeiitic and mildly alkaline magmatic systems. *Contributions to Mineralogy and Petrology*, *135*(1), 62–74.
Nimis, P., & Taylor, W. R. (2000). Single clinopyroxene thermobarometry for garnet peridotites. Part I. Calibration and testing of a Cr-in-Cpx barometer and an enstatite-in-Cpx thermometer. *Contributions to Mineralogy and Petrology*, *139*(5), 541–554.
Niu, Y. (1997). Mantle melting and melt extraction processes beneath ocean ridges: Evidence from abyssal peridotites. *Journal of Petrology*, *38*(8), 1047–1074.
Niu, Y. (2005). Generation and evolution of basaltic magmas: Some basic concepts and a new view on the origin of Mesozoic–Cenozoic basaltic volcanism in eastern China. *Geological Journal of China Universities*, *11*(1), 9–46.
Niu, Y. (2008). The origin of alkaline lavas. *Science*, *320*(5878), 883–884. https://doi.org/10.1126/science.1158378
Niu, Y. (2016). The meaning of global ocean ridge basalt major element compositions. *Journal of Petrology*, *57*(11–12), 2081–2103.
Niu, Y., & Batiza, R. (1991). An empirical method for calculating melt compositions produced beneath mid-ocean ridges: Application for axis and off-axis (seamounts) melting. *Journal of Geophysical Research*, *96*(B13), 21,753–21,777.
Niu, Y., Collerson, K. D., Batiza, R., Wendt, J. I., & Regelous, M. (1999). Origin of enriched-type mid-ocean ridge basalt at ridges far from mantle plumes: The East Pacific Rise at 11°20′N. *Journal of Geophysical Research*, *104*(B4), 7067–7087.
Niu, Y., & Green, D. H. (2018). The petrological control on the lithosphere-asthenosphere boundary (LAB) beneath ocean basins. *Earth-Science Reviews*, *185*, 301–307.
Niu, Y., Liu, Y., Xue, Q., Shao, F., Chen, S., Duan, M., et al. (2015). Exotic origin of the Chinese continental shelf: New insights into the tectonic evolution of the western Pacific and eastern China since the Mesozoic. *Science Bulletin*, *60*(18), 1598–1616.
Niu, Y., & O'Hara, M. J. (2008). Global correlations of ocean ridge basalt chemistry with axial depth: A new perspective. *Journal of Petrology*, *49*(4), 633–664.
Niu, Y., & O'Hara, M. J. (2009). MORB mantle hosts the missing Eu (Sr, Nb, ta and Ti) in the continental crust: New perspectives on crustal growth, crust–mantle differentiation and chemical structure of oceanic upper mantle. *Lithos*, *112*(1), 1–17.
Niu, Y., Waggoner, D. G., Sinton, J. M., & Mahoney, J. J. (1996). Mantle source heterogeneity and melting processes beneath seafloor spreading centers: The East Pacific Rise, 18–19 S. *Journal of Geophysical Research*, *101*(B12), 27,711–27,733.
Niu, Y., Wilson, M., Humphreys, E. R., & O'Hara, M. J. (2011). The origin of intra-plate ocean island basalts (OIB): The lid effect and its geodynamic implications. *Journal of Petrology*, *52*(7–8), 1443–1468.
Niu, Y., Wilson, M., Humphreys, E. R., & O'Hara, M. J. (2012). A trace element perspective on the source of ocean island basalts (OIB) and fate of subducted ocean crust (SOC) and mantle lithosphere (SML). *Episodes*, *35*(2), 310–327.
O'Hara, M. J. (1965). Primary magmas and the origin of basalts. *Scottish Journal of Geology*, *1*(1), 19–40.
Parsons, B., & McKenzie, D. (1978). Mantle convection and the thermal structure of the plates. *Journal of Geophysical Research*, *83*(B9), 4485–4496.
Peng, Z., Zartman, R., Futa, K., & Chen, D. (1986). Pb-, Sr-and Nd-isotopic systematics and chemical characteristics of Cenozoic basalts, eastern China. *Chemical Geology: Isotope Geoscience Section*, *59*, 3–33.
Putirka, K., Johnson, M., Kinzler, R., Longhi, J., & Walker, D. (1996). Thermobarometry of mafic igneous rocks based on clinopyroxene-liquid equilibria, 0–30 kbar. *Contributions to Mineralogy and Petrology*, *123*(1), 92–108.
Putirka, K. D. (2005). Mantle potential temperatures at Hawaii, Iceland, and the mid-ocean ridge system, as inferred from olivine phenocrysts: Evidence for thermally driven mantle plumes. *Geochemistry, Geophysics, Geosystems*, *6*, Q05L08. https://doi.org/10.1029/2005GC000915
Putirka, K. D. (2008). Thermometers and barometers for volcanic systems. *Reviews in Mineralogy and Geochemistry*, *69*(1), 61–120.
Putirka, K. D., Mikaelian, H., Ryerson, F., & Shaw, H. (2003). New clinopyroxene-liquid thermobarometers for mafic, evolved, and volatile-bearing lava compositions, with applications to lavas from Tibet and the Snake River Plain, Idaho. *American Mineralogist*, *88*(10), 1542–1554.
Qi, Q., Taylor, L. A., & Zhou, X. (1994). Geochemistry and petrogenesis of three series of Cenozoic basalts from southeastern China. *International Geology Review*, *36*(5), 435–451.
Richter, K., & Carmichael, I. S. E. (1993). Mega-xenocrysts in alkali olivine basalts: Fragments of disrupted mantle assemblages. *American Mineralogist*, *78*(11-12), 1230–1245.
Roeder, P., & Emslie, R. (1970). Olivine-liquid equilibrium. *Contributions to Mineralogy and Petrology*, *29*(4), 275–289.
Sakuyama, T., Tian, W., Kimura, J. I., Fukao, Y., Hirahara, Y., Takahashi, T., et al. (2013). Melting of dehydrated oceanic crust from the stagnant slab and of the hydrated mantle transition zone: Constraints from Cenozoic alkaline basalts in eastern China. *Chemical Geology*, *359*, 32–48. https://doi.org/10.1016/j.chemgeo.2013.09.012

Schmerr, N. (2012). The Gutenberg discontinuity: Melt at the lithosphere-asthenosphere boundary. *Science*, *335*(6075), 1480–1483. https://doi.org/10.1126/science.1215433

Sclater, J. G., & Francheteau, J. (1970). The implications of terrestrial heat flow observations on current tectonic and geochemical models of the crust and upper mantle of the Earth. *Geophysical Journal International*, *20*(5), 509–542.

Shan, B., Xiong, X., Zhao, K. F., Xie, Z. J., Zheng, Y., & Zhou, L. (2016). Crustal and upper-mantle structure of South China from Rayleigh wave tomography. *Geophysical Journal International*, *208*(3), 1643–1654.

Shaw, C. S., & Eyzaguirre, J. (2000). Origin of megacrysts in the mafic alkaline lavas of the West Eifel volcanic field, Germany. *Lithos*, *50*(1), 75–95.

Song, Y., Frey, F. A., & Zhi, X. (1990). Isotopic characteristics of Hannuoba basalts, eastern China: Implications for their petrogenesis and the composition of subcontinental mantle. *Chemical Geology*, *88*(1), 35–52.

Stolper, E. (1980). A phase diagram for mid-ocean ridge basalts: Preliminary results and implications for petrogenesis. *Contributions to Mineralogy and Petrology*, *74*(1), 13–27.

Su, F., Xiao, Y., He, H., Su, B., Wang, Y., & Zhu, R. (2014). He and Ar isotope geochemistry of pyroxene megacrysts and mantle xenoliths in Cenozoic basalt from the Changle–Linqu area in western Shandong. *Chinese Science Bulletin*, *59*(4), 396–411.

Sun, P., Niu, Y., Guo, P., Chen, S., Duan, M., Gong, H., et al. (2019). Multiple mantle metasomatism beneath the Leizhou Peninsula, South China: Evidence from elemental and Sr-Nd-Pb-Hf isotope geochemistry of the late Cenozoic volcanic rocks. *International Geology Review*, *61*(14), 1768–1785.

Sun, P., Niu, Y., Guo, P., Cui, H., Ye, L., & Liu, J. (2018). The evolution and ascent paths of mantle xenolith-bearing magma: Observations and insights from Cenozoic basalts in Southeast China. *Lithos*, *310-311*, 171–181.

Sun, P., Niu, Y., Guo, P., Ye, L., Liu, J., & Feng, Y. (2017). Elemental and Sr–Nd–Pb isotope geochemistry of the Cenozoic basalts in Southeast China: Insights into their mantle sources and melting processes. *Lithos*, *272-273*, 16–30.

Tamura, Y., Yuhara, M., & Ishii, T. (2000). Primary arc basalts from Daisen Volcano, Japan: Equilibrium crystal fractionation versus disequilibrium fractionation during supercooling. *Journal of Petrology*, *41*(3), 431–448.

Tharimena, S., Rychert, C., & Harmon, N. (2017). A unified continental thickness from seismology and diamonds suggests a melt-defined plate. *Science*, *357*(6351), 580–583. https://doi.org/10.1126/science.aan0741

Tu, K., Flower, M. F., Carlson, R. W., Zhang, M., & Xie, G. (1991). Sr, Nd, and Pb isotopic compositions of Hainan basalts (south China): Implications for a subcontinental lithosphere Dupal source. *Geology*, *19*(6), 567–569.

Walter, M. J. (1998). Melting of garnet peridotite and the origin of komatiite and depleted lithosphere. *Journal of Petrology*, *39*(1), 29–60.

Wang, X.-C., Li, Z.-X., Li, X.-H., Li, J., Liu, Y., Long, W.-G., et al. (2011). Temperature, pressure, and composition of the mantle source region of late Cenozoic basalts in Hainan Island, SE Asia: A consequence of a young thermal mantle plume close to subduction zones? *Journal of Petrology*, *53*(1), 177–233.

Wang, Y. (2011). Quaternary volcanic activity and the new structure, Xilinhot, Inner Mogilia. MD thesis, China University of Geosciences.

Wang, Y., Zhao, Z.-F., Zheng, Y.-F., & Zhang, J.-J. (2011). Geochemical constraints on the nature of mantle source for Cenozoic continental basalts in east-central China. *Lithos*, *125*(3), 940–955.

Wass, S. Y. (1979). Multiple origins of clinopyroxenes in alkali basaltic rocks. *Lithos*, *12*(2), 115–132.

White, W. M., & Hofmann, A. W. (1982). Sr and Nd isotope geochemistry of oceanic basalts and mantle evolution. *Nature*, *296*, 821–825.

Wilshire, H. G., & Shervais, J. W. (1975). Al-augite and Cr-diopside ultramafic xenoliths in basaltic rocks from western United States. In L. H. Ahrens, J. B. Dawson, A. R. Duncan, & A. J. Erlank (Eds.), *Physics and chemistry of the earth* (pp. 257–272). New York: Pergamon.

Woodland, A., & Jugo, P. (2007). A complex magmatic system beneath the Deves volcanic field, Massif Central, France: Evidence from clinopyroxene megacrysts. *Contributions to Mineralogy and Petrology*, *153*(6), 719–731.

Wu, F.-Y., Walker, R. J., Yang, Y.-H., Yuan, H.-L., & Yang, J.-H. (2006). The chemical-temporal evolution of lithospheric mantle underlying the North China Craton. *Geochimica et Cosmochimica Acta*, *70*(19), 5013–5034.

Xia, Q.-K., Dallai, L., & Deloule, E. (2004). Oxygen and hydrogen isotope heterogeneity of clinopyroxene megacrysts from Nushan Volcano, SE China. *Chemical Geology*, *209*(1), 137–151.

Xu, X., O'Reilly, S. Y., Griffin, W., & Zhou, X. (2000). Genesis of young lithospheric mantle in Southeastern China: An LAM–ICPMS trace element study. *Journal of Petrology*, *41*(1), 111–148.

Xu, Z., Zhao, Z.-F., & Zheng, Y.-F. (2012). Slab–mantle interaction for thinning of cratonic lithospheric mantle in North China: Geochemical evidence from Cenozoic continental basalts in central Shandong. *Lithos*, *146-147*, 202–217.

Yang, R., Bai, Z., Tan, Q., Wu, Z., & Wang, Y. (2012). Study on the geology of Gezi Shan volcano in Xilinhot, Inner Mongolia (in Chinese with English abstract). *Acta Petrologica Sinica*, *28*(4), 1181–1188.

Yoder, H. S. Jr. (1965). Diopside-anorthite-water at five and ten kilobars and its bearing on explosive volcanism. *Carnegie Institution of Washington Yearbook*, *64*, 82–89.

Yu, X., Zeng, G., Chen, L.-H., Hu, S.-L., & Yu, Z.-Q. (2019). Magma–magma interaction in the mantle recorded by megacrysts from Cenozoic basalts in eastern China. *International Geology Review*, *61*(6), 675–691.

Zhang, M., Suddaby, P., Thompson, R. N., Thirlwall, M. F., & Menzies, M. A. (1995). Potassic volcanic rocks in NE China: Geochemical constraints on mantle source and magma genesis. *Journal of Petrology*, *36*(5), 1275–1303.

Zheng, Y., Shen, W., Zhou, L., Yang, Y., Xie, Z., & Ritzwoller, M. H. (2011). Crust and uppermost mantle beneath the North China Craton, northeastern China, and the Sea of Japan from ambient noise tomography. *Journal of Geophysical Research*, *116*, B12312. https://doi.org/10.1029/2011JB008637

Zindler, A., & Hart, S. (1986). Chemical geodynamics. *Annual Review of Earth and Planetary Sciences*, *14*, 493–571.

Zou, H., Zindler, A., Xu, X., & Qi, Q. (2000). Major, trace element, and Nd, Sr and Pb isotope studies of Cenozoic basalts in SE China: Mantle sources, regional variations, and tectonic significance. *Chemical Geology*, *171*(1), 33–47.

References From the Supporting Information

Liu, Y., Hu, Z., Gao, S., Günther, D., Xu, J., Gao, C., & Chen, H. (2008). In situ analysis of major and trace elements of anhydrous minerals by LA-ICP-MS without applying an internal standard. *Chemical Geology*, *257*(1–2), 34–43.

Song, S., Su, L., Li, X.-h., Zhang, G., Niu, Y., & Zhang, L. (2010). Tracing the 850-Ma continental flood basalts from a piece of subducted continental crust in the North Qaidam UHPM belt, NW China. *Precambrian Research*, *183*(4), 805–816.

Sun, S.-S., & McDonough, W. (1989). Chemical and isotopic systematics of oceanic basalts: Implications for mantle composition and processes. *Geological Society, London, Special Publications*, *42*(1), 313–345.

Zack, T., Foley, S. F., & Jenner, G. A. (1997). A consistent partition coefficient set for clinopyroxene, amphibole and garnet from laser ablation microprobe analysis of garnet pyroxenites from Kakanui, New Zealand. *Neues Jahrbuch für Mineralogie (Abhandlungen)*, 23–41.